Journal of NUCLEAR SCIENCE and TECHNOLOGY, Vol. 39, No. 1, p. 101–107 (January 2002)

TECHNICAL REPORT

Analytical Study of Volumetric Scroll Pump for Liquid Hydrogen Circulating System

Phichai KRITMAITREE[1], Mitsunobu AKIYAMA[1], Ryutaro HINO[2,*], Masanori KAMINAGA[2] and Atsuhiko TERADA[2]

[1]*Mechanical Engineering Department, Utsunomiya University, 2753 Ishii-machi, Utsunomiya-shi, Tochigi 321-0912*
[2]*System Engineering Group, Tokai Research Establishment, Japan Atomic Energy Research Institute, 2-4 Shirakata-Shirane, Tokai-mura, Naka-gun, Ibaraki 319-1195*

(Received August 24, 2001 and accepted October 29, 2001)

The paper presents analytical results of suction process of a volumetric scroll pump, which will be developed for circulating liquid hydrogen in a cold moderator system. The multi-block grid generation approach has been applied to generate a moving boundaries computational model. The finer mesh patterns have been generated in the near-wall regions. The Low-Reynolds number k-ε turbulence model has been solved for predicting Reynolds stresses and turbulent scalar fluxes. The analysis has been carried out under liquid hydrogen flow conditions. The heat transfer effect is neglected to simplify the study. The analytical results show that at the end of suction process the relative pressures increase significantly in a pocket while decrease continuously in another pocket. This phenomenon might damage scroll pump components if the high-pressure side is too high and/or the low-pressure side is too low until the cavitations occur. Therefore, the pocket should open to the discharge chamber before it closes and separates from the suction chamber in order to prevent the cavitations and extremely high-pressure regions.

KEYWORDS: volumetric scroll pump, liquid hydrogen, suction process, circulating systems, pressure distribution, velocity distribution, pressure dependence

I. Introduction

The volumetric scroll pump has been studied for a cold moderator system, which is one of key components of a MW-class spallation neutron source research and development at Japan Atomic Energy Research Institute (JAERI) since 2000.[1)] An appropriate and safety operation could be expected in its application with the cold moderator system due to the volumetric pump features, *i.e.* two-phase flow capability, low speed, small size, and proportional flow rate control.[1,2)] At present, the design of the scroll pump components in an application of liquid hydrogen circulating system is still a very difficult task. The primary purpose of the analytical study is to understand the fluid flow behavior inside the scroll pump. Thereafter, an experiment would be performed in a proper way so that the reliable results could be expected.

In the previous study, the scroll pump has been developed and analyzed numerically to predict flow patterns and pressure distributions in the suction process under water conditions.[1)] The results showed that the scroll pump had small negative relative pressure, and preferable volumetric intake profile. The previous study has also illustrated that at the end of the suction process the relative pressure increases significantly in a suction pocket, *i.e.* the region between the orbiting and the fixed scroll wrap, and decreases continuously in another pocket.[2)]

In the present study, we mainly concentrate on the solution at the positions close to the end of the suction process. The analytical model has been reconstructed for predicting flow patterns and pressure distributions in the suction process under liquid hydrogen conditions at 20 K and atmospheric pressure at suction inlet. The improvements of the analytical model are scroll model parameters, cell connectivity, cell shape, cell size and time step.

*Corresponding author; Tel. +81-029-282-5145, Fax. +81-029-282-6496, E-mail: hino@cat.tokai.jaeri.go.jp

II. Analytical Model

The processes inside the scroll pump are as illustrated in **Fig. 1** and the scroll pump configuration is as shown in **Fig. 2**. The coordinate equations of the perimeter curves of the scrolls are as follows:

Fixed scroll

Inner curve
$$X = \alpha(\cos\lambda + (\lambda + \pi - \beta)\sin\lambda)$$
$$Y = \alpha(\sin\lambda - (\lambda + \pi - \beta)\cos\lambda)$$
$$0 \le \lambda \le 3\pi$$

Outer curve
$$X = \alpha(\cos\lambda + (\lambda - \pi)\sin\lambda)$$
$$Y = \alpha(\sin\lambda - (\lambda - \pi)\cos\lambda)$$
$$2\pi \le \lambda \le 5\pi$$

Orbiting scroll

Inner curve
$$X = \alpha(\cos\lambda + (\lambda - \beta)\sin\lambda) + \gamma\cos\theta$$
$$Y = \alpha(\sin\lambda - (\lambda - \beta)\cos\lambda) + \gamma\sin\theta$$
$$\pi \le \lambda \le 4\pi$$

Outer curve
$$X = \alpha(\cos\lambda + \lambda\sin\lambda) + \gamma\cos\theta$$
$$Y = \alpha(\sin\lambda - \lambda\cos\lambda) + \gamma\sin\theta$$
$$\pi \le \lambda \le 4\pi$$

where α: Scroll coefficient (mm)
β: Discrepancy of starting rolls angle (radian)
γ: Radius of basic circle, $\alpha(\pi - \beta)$ (radian)
θ: Crank angle (radian)
λ: Position angle (radian).

Adjustment of scroll coefficient α would change the scroll

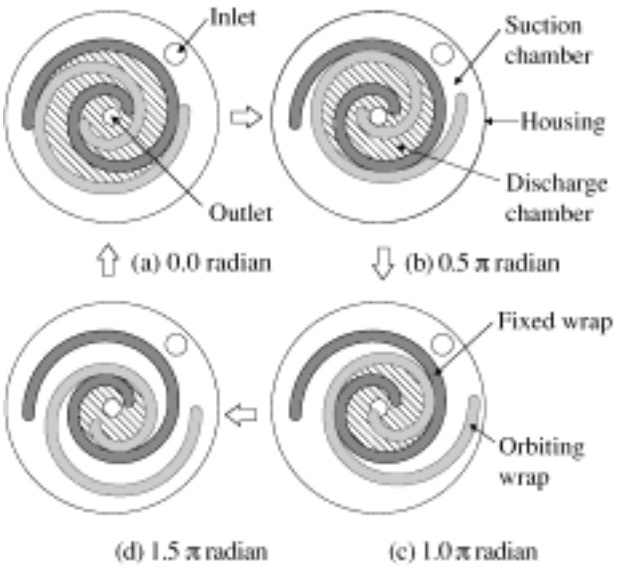

Fig. 1 Process inside a scroll pump

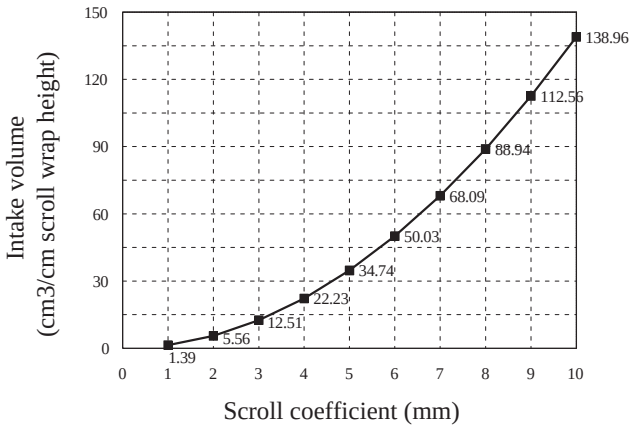

Fig. 3 Relationship between intake volume and scroll coefficient α (β=0.5π radian)

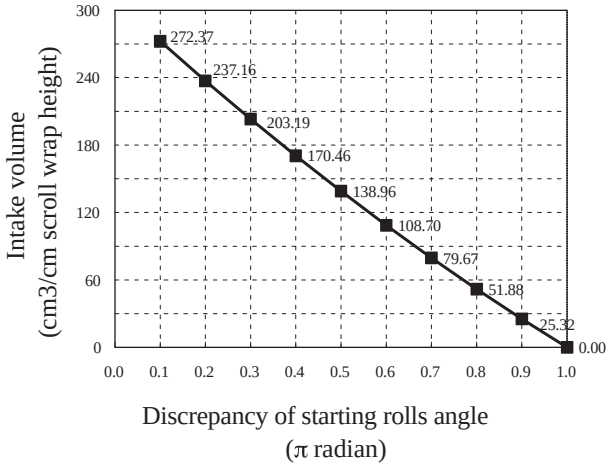

Fig. 4 Relationship between intake volume and discrepancy of starting roll angles β

pump size in scale while adjustment of discrepancy of starting rolls angle β would change the shape of the scroll wraps (*i.e.* changing the thickness of scroll wraps). The comparison of the scroll models in different values of β is also shown in Fig. 2. The relationship between intake volume and scroll coefficient α is shown in **Fig. 3**, while the relationship between intake volume and discrepancy of starting rolls angle β is shown in **Fig. 4**. Therefore, it could confirm that scroll pump can be designed and configured before applying to the circulation system to meet the flow rate condition of the system. In the study, the scroll coefficient and the discrepancy of starting rolls angle are set to 5 mm and 0.5π radian, respectively, resulting the analytical model which has an appropriate pump size of 149.2 mm in diameter and 50 mm in depth, the suction port has its diameter of 15.7 mm and its center at X=46.2 mm; Y=−42.7 mm, while the discharge port has its diameter of 11.8 mm and its center at X=6.3 mm; Y=0.8 mm. The inlet and outlet pipes have the same diameter as the connecting ports with each of 50 mm in length.

The three-dimensional fluid cells model of the scroll pump is generated by using multi-block grid generation approach.[3] This approach is provided in PROSTAR, the pre- and post-processing subsystems of the STAR-CD thermal-hydraulic analytical codes. The computational domain is firstly divided into simple individual regions, which are so-called blocks. The edges of the three-dimensional blocks are created by importing vertices and splines input data. In the study, the input data were calculated from the scroll configuration equations described above for 72 time steps of $\frac{1}{36}\pi$ radian of crank angle. To treat a moving boundary problem, therefore the blocks are separated into two groups, *i.e.*, the deformed shape and the fixed shape blocks. The moving meshes were generated inside the deformed blocks repeatedly at each time step while the fixed meshes were generated inside the fixed blocks. With a well-designed consideration, the blocks inside the pump are connected by common perimeter surfaces, except the connecting pipe to the pump. Assigning the same number and distribution of cells on any common perimeter surfaces would give good connectivity cells. Therefore, the arbitrary mesh interface technique is required only for matching the cells of connecting pipe to the cells of the pump. To meet the requirement of the Low-Reynolds number k-ε turbulence model the finer mesh patterns would be generated in the near-wall regions. The resulting cells in several steps in plane view are shown in **Fig. 5**. The cells must be managed to activate or deactivate along with their position changed at each step of calculation. The active cells are 97,200 cells at the first step then activate 800 cells into the cell set at each time step resulting of 154,000 cells at the last step. Note that, in the previous study, they have been set at 9,410 cells and 16,760 at the first and the last step, respectively.

The analysis was carried out under liquid hydrogen flow conditions. The heat transfer effect is neglected to simplify the study. Therefore, the temperature, density, molecular viscosity, specific heat, and thermal conductivity of the liquid hydrogen are held constant at 20 K, 70.8 kg/m^3, 1.37×10^{-5} kg/ms, 1.02×10^4 J/kg·K, and 0.1 W/m·K, respectively. Note that the average Reynolds number at the suction inlet is about 24,340. The flow is assumed to be tur-

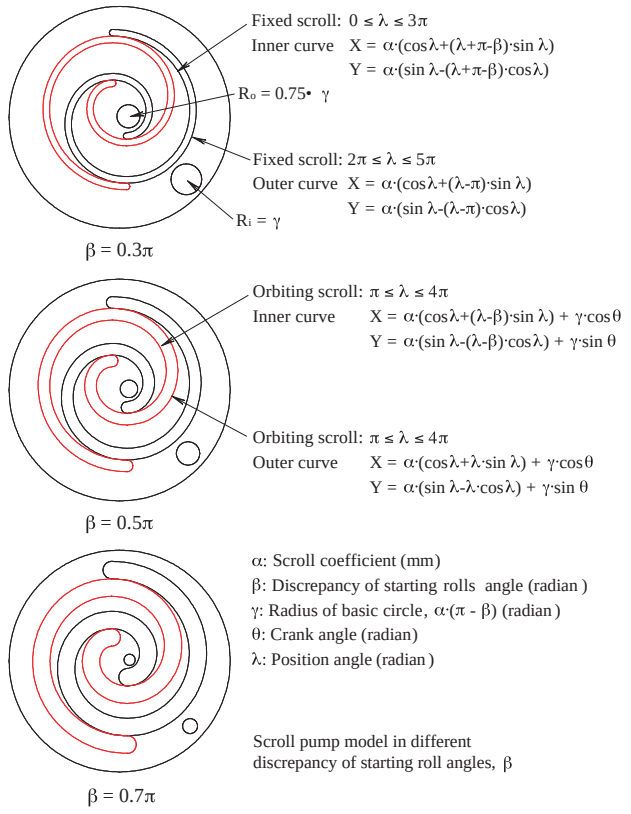

Fig. 2 Scroll pump configuration

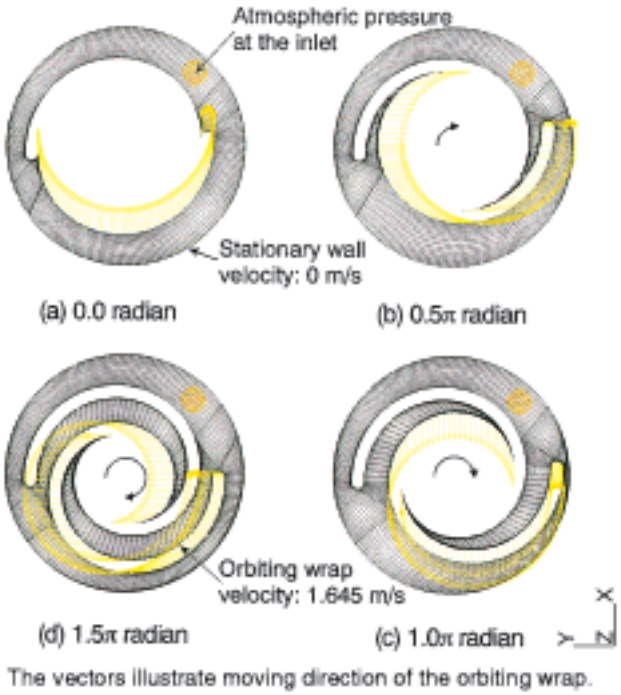

Fig. 5 Computational grid of the scroll pump

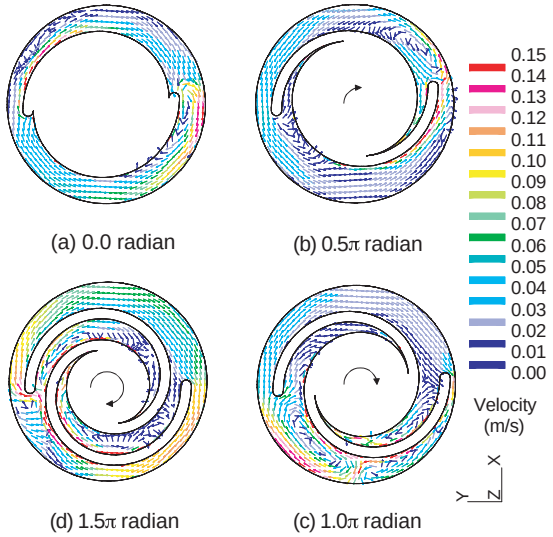

Fig. 7 Velocity vector at several angles

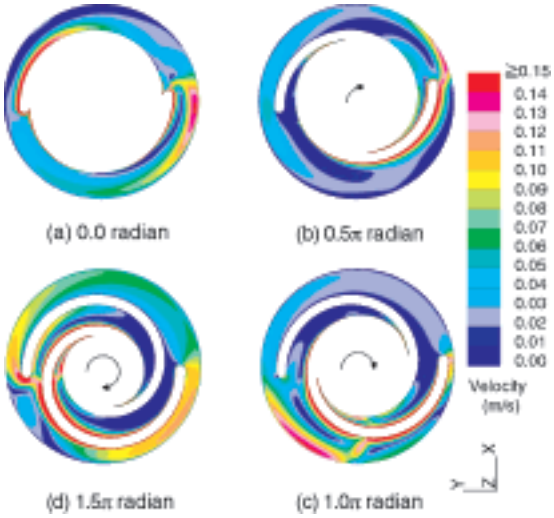

Fig. 8 Velocity contour at several angles

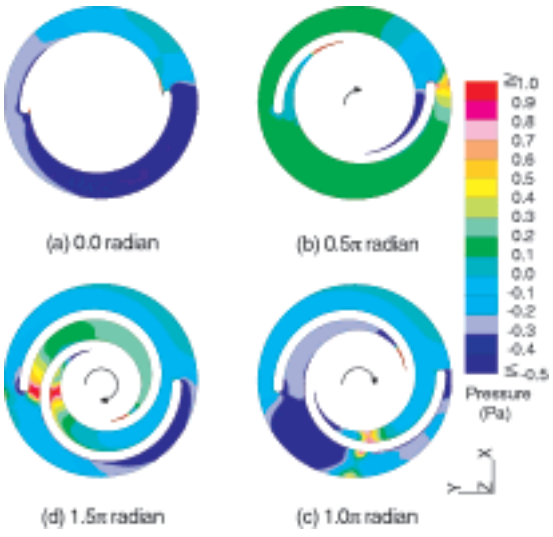

Fig. 9 Static pressure distribution at several angles

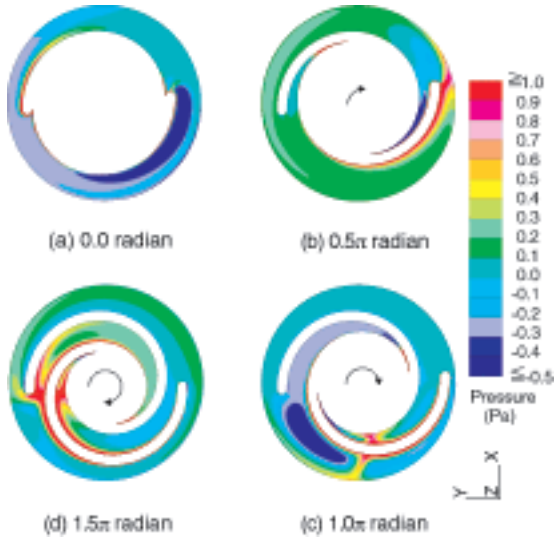

Fig. 10 Total pressure distribution at several angles

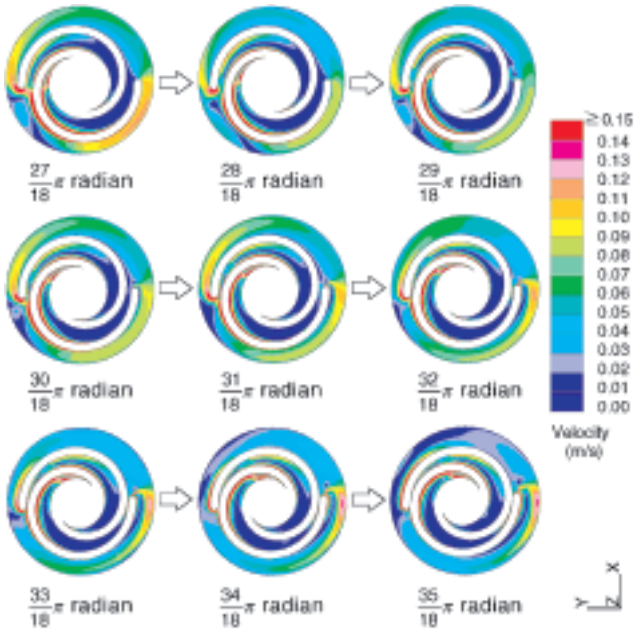

Fig. 11 Velocity contour in the last quarter

bulent and induced by the motion of the orbiting scroll wrap. The Low-Reynolds number k-ε turbulence model was applied to determine the Reynolds stress and turbulent scalar fluxes. The suction inlet port boundary pressures are held constant at atmospheric pressure boundary condition throughout the computation. The velocity magnitude of the orbiting scroll equals to 1.645 m/s according to the shaft speed of 2,000 rpm. The illustrations of the boundary conditions are also shown in Fig. 5.

III. Mathematical Model

The mass and momentum conservation equations for general incompressible and compressible fluids flows with a moving coordinate frame (the Navier-Stokes equations) are, in Cartesian tensor notation:

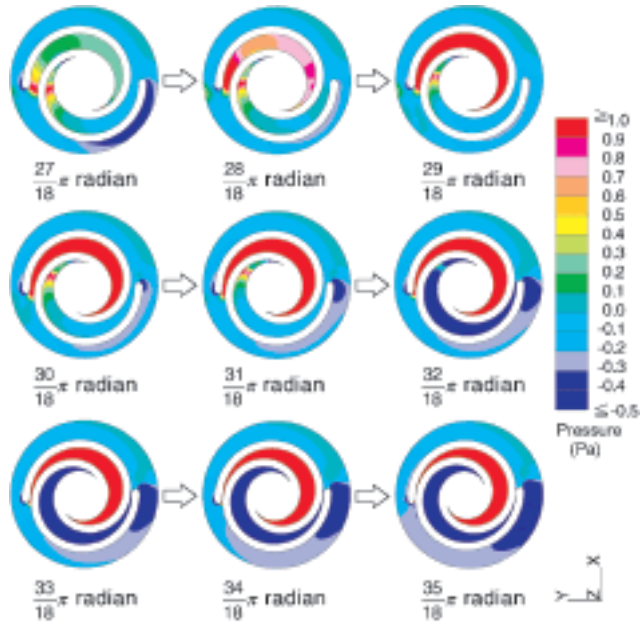

Fig. 12 Static pressure distribution in the last quarter

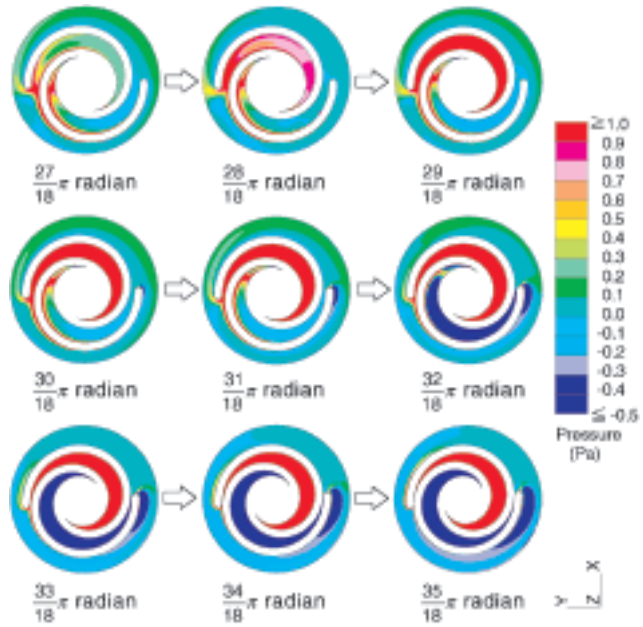

Fig. 13 Total pressure distribution in the last quarter

$$\frac{1}{\sqrt{g}} \cdot \frac{\partial}{\partial t}(\sqrt{g}\rho) + \frac{\partial}{\partial x_j}(\rho \tilde{u}_j) = s_m \tag{1}$$

$$\frac{1}{\sqrt{g}} \cdot \frac{\partial}{\partial t}(\sqrt{g}\rho u_i) + \frac{\partial}{\partial x_j}(\rho \tilde{u}_j u_i - \tau_{ij}) = -\frac{\partial p}{\partial x_i} + s_i, \tag{2}$$

where $\sqrt{g}$: Determinant of metric tensor
p: Piezometric pressure$=p_s-\rho_0 g_m x_m$ where p_s is the static pressure, ρ_0 is the reference density, g_m are gravitational field components and x_m are coordinates from a datum, where ρ_0 is defined

s_i: Momentum source components
s_m: Mass source
t: Time
u_i: Absolute fluid velocity component in direction x_i
$\tilde{u}_j$: relative velocity between fluid and local (moving) coordinate frame that moves with velocity u_{cj}, $u_j - u_{cj}$
x_i: Cartesian coordinate (i=1, 2, 3)
ρ: Density
τ_{ij}: Stress tensor components.

For turbulent flows u_i, p and other dependent variables, including τ_{ij}, assume their ensemble average values giving, for Newtonian fluids:

$$\tau_{ij} = 2\mu s_{ij} - \frac{2}{3}\mu\frac{\partial u_k}{\partial x_k}\delta_{ij} - \bar{\rho}\overline{u_i' u_j'}, \tag{3}$$

where μ is the molecular dynamic fluid viscosity and δ_{ij}, the 'Kronecker delta', is unity when i=j and zero otherwise, s_{ij}, the rate of strain tensor, is given by

$$s_{ij} = \frac{1}{2}\left(\frac{\partial u_i}{\partial x_j} + \frac{\partial u_j}{\partial x_i}\right), \tag{4}$$

u' are fluctuations about the ensemble average velocity and the overbar denotes the ensemble averaging process. The term $-\bar{\rho}\overline{u_i' u_j'}$ in the above represents the additional Reynolds stresses due to turbulent motion. By assuming that the Reynolds stresses are linked to the ensemble average flow properties in an analogous to their laminar flow counterparts, thus:

$$-\bar{\rho}\overline{u_i' u_j'} = 2\mu_t s_{ij} - \frac{2}{3}\left(\mu_t\frac{\partial u_k}{\partial x_k} + \rho k\right)\delta_{ij}, \tag{5}$$

where $k \equiv \overline{u_i' u_i'}/2$ is the turbulent kinetic energy, and μ_t is the turbulent viscosity.

In this study, these turbulent properties are determined by introducing the Low-Reynolds number k-ε turbulence model. The Low-Reynolds number model in which general transport equations for k and ε are solved everywhere, including the near-wall regions.[4] The transport equations of the Low-Reynolds number k-ε turbulence model are as follows:
Turbulence energy

$$\frac{1}{\sqrt{g}}\cdot\frac{\partial}{\partial t}(\sqrt{g}\rho k) + \frac{\partial}{\partial x_j}\left(\rho\tilde{u}_j k - \frac{\mu_{\text{eff}}}{\sigma_k}\cdot\frac{\partial k}{\partial x_j}\right) = \mu_t(P - P_B) - \rho\varepsilon - \frac{2}{3}\left(\mu_t\frac{\partial u_i}{\partial x_i} + \rho k\right)\frac{\partial u_i}{\partial x_i}, \tag{6}$$

where

$$\mu_{\text{eff}} = \mu + \mu_t \tag{7}$$

$$P \equiv 2 s_{ij}\frac{\partial u_i}{\partial x_j} \tag{8}$$

$$P_B \equiv -\frac{g_i}{\sigma_{h,t}}\cdot\frac{1}{\rho}\cdot\frac{\partial \rho}{\partial x_i}. \tag{9}$$

The first term on the right-hand side of the turbulence energy equation represents turbulent generation by shear and normal stresses and buoyancy forces, the second viscous dissipation, and the third amplification or attenuation due to compressibility effects.

Turbulence dissipation rate

$$\frac{1}{\sqrt{g}}\cdot\frac{\partial}{\partial t}(\sqrt{g}\rho\varepsilon) + \frac{\partial}{\partial x_j}\left(\rho\tilde{u}_j\varepsilon - \frac{\mu_{\text{eff}}}{\sigma_\varepsilon}\cdot\frac{\partial\varepsilon}{\partial x_j}\right) = C_{\varepsilon 1}\frac{\varepsilon}{k}\left[\mu_t(P + P') - \frac{2}{3}\left(\mu_t\frac{\partial u_i}{\partial x_i} + \rho k\right)\frac{\partial u_i}{\partial x_i}\right] + C_{\varepsilon 3}\frac{\varepsilon}{k}\mu_t P_B - C_{\varepsilon 2}(1 - 0.3e^{-R_t^2})\rho\frac{\varepsilon^2}{k} + C_{\varepsilon 4}\rho\varepsilon\frac{\partial u_i}{\partial x_i}, \tag{10}$$

where σ_k, σ_ε, $C_{\varepsilon 1}$, $C_{\varepsilon 2}$, $C_{\varepsilon 3}$ and $C_{\varepsilon 4}$ are empirical coefficients whose values are 1.0, 1.22, 1.44, 1.92, 0.0 (1.44 for P_B>0), and -0.33 respectively.[5,6] The right-hand side terms of the above represents analogous effects to those described above for the turbulence energy equation.
P' is given by

$$P' = 1.33[1 - 0.3e^{-R_t^2}]\left(P + 2\frac{\mu}{\mu_t}\cdot\frac{k}{y^2}\right)e^{-0.00375 Re_y^2}. \tag{11}$$

The turbulent viscosity μ_t, appearing in the above, is linked to k and ε *via*:

$$\mu_t = f_\mu\frac{C_\mu\rho k^2}{\varepsilon} \tag{12}$$

with f_μ given by

$$f_\mu = [1 - 0.3e^{-0.0198 Re_y}]\left(1 + \frac{5.29}{Re_y}\right) \tag{13}$$

in which

$$Re_y = \frac{y\sqrt{k}}{v}. \tag{14}$$

The turbulent Reynolds number R_t is given by

$$R_t = \frac{k^2}{v\varepsilon}. \tag{15}$$

The differential equations governing mentioned above, are discretised by the finite volume method and solve by PISO algorithm.[7]

IV. Results and Discussions

The intake volume profile has been plotted with the corresponding angle in **Fig. 6**. These values have been calculated by subtracting the total cell volume at the first step (zero radian) from the total cell volume at each time steps. In the figure, the approximate intake volume of one cycle (2π radian) is 174 cm^3. This value could also be estimated from Fig. 3, which has the intake volume equals to 34.74 cm^3 per cm of scroll height. This would give the volume flow rate of 5.8 *l*/s at 2,000 rpm or 1.0 *l*/s at 345 rpm. In this case, adjusting the crank speed could control the fluid flow rate of the system.

In the following discussion, the analytical results of liquid hydrogen flow in the suction process would be plotted on the center section surface, z=25 mm, in several positions. Corresponding to Fig. 1, the results of velocity vector, velocity magnitude, static pressure and total pressure are plotted at 0.0, 0.5π, 1.0π, and 1.5π radian in **Figs. 7** to **10**, respectively. The pressures are relative pressures, which indicate the

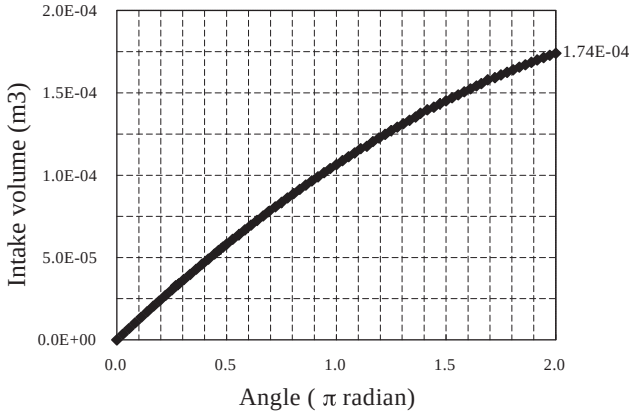

Fig. 6 Intake volume profile of suction process

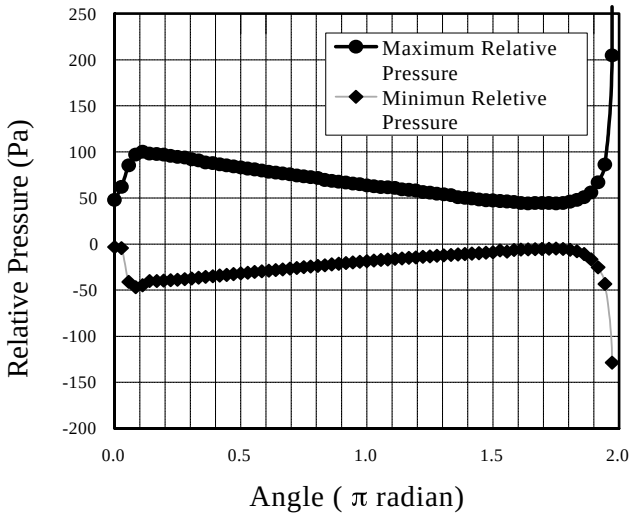

Fig. 14 Maximum and minimum relative pressure plot at several angles

pressures difference against the inlet pressure.

The velocity results in Figs. 7 and 8 show how the orbiting scroll induces velocity fields. In the figures, the orbiting wrap drives the surrounding fluid and induces the high velocity fields nearby the wrap in its moving direction. It can be seen that the recirculation flows occur in the regions where the high velocity fluids flow against the stationary wall. The impaction of the high velocity fluids buildup the other high velocity regions near the stationary wall. Refer to the previous study; the momentum exchange through the liquid hydrogen is less than the case of water since liquid hydrogen has very low density comparing with water.

In Fig. 9, the static pressure results show that low pressure occurs in the regions that the orbiting scroll moves from while high pressure occurs in the regions that the orbiting scroll moves to. It can be seen in the figure that, the impaction of the high velocity fluids also buildup the high static pressure regions between the orbiting wrap and stationary wall where the recirculation flows occur. In Fig. 10, the total pressure results summarized the dynamic pressure and the static pressure of the liquid hydrogen. The high-pressure regions are the regions that the dynamic and the static pressure are high, *i.e.* the regions surrounding the orbiting wrap and the regions that the recirculation flows occur. The figure also shows that the composition of the dynamic and the static pressure gives smoother contours comparing with the dynamic or the static pressure contours.

The results of velocity magnitude, static pressure and total pressure have been plotted again to see how these flow properties change in the last quarter of the suction process using $\frac{1}{18}\pi$-radian step from $\frac{27}{18}\pi$ to $\frac{35}{18}\pi$ radian in **Figs. 11** to **13**, respectively.

In Figs. 11 to 13, the results agree with the discussion above as well. However, it can be noticed that the relative pressures increase significantly in a pocket while decrease continuously in another pocket. As seen in the figures, the change mainly happens to static pressure distributions due to the orbiting wrap moves to close the pockets. The high-pressure pocket is where the fluid inside attempts to flow out and the low-pressure pocket is where the fluid outside attempts to flow into. This phenomenon might damage scroll pump components if the high-pressure side is too high and/or the low-pressure side is too low until the cavitations occur. In ideal case, when the pocket closes and separates fluid inside from suction chamber, it also opens fluid inside to discharge chamber at same time. Therefore, as seen in the analytical results, to prevent the cavitations and extremely high-pressure regions, the pocket should open to the discharge chamber before it closes and separates from the suction chamber. For the purpose, the maximum and minimum values of total pressure are plotted with the corresponding angle in **Fig. 14**.

It can be noticed in Fig. 14 that the maximum and minimum pressures are mirror image of each other. Therefore, the position that has high maximum value also has low minimum valve. In the figure, the highest maximum and the lowest minimum would be at 2π radian. In the analytical results, the acceptable values are at $\frac{71}{36}\pi$ radian where the maximum relative pressure is equal to 205 Pa and the minimum relative pressure is equal to -129 Pa. The cavitations would not occur with this minimum relative pressure in an application to sub-cooled liquid hydrogen at 20 K and 1.5 MPa at suction inlet.

V. Concluding Remarks

The numerical analysis in the suction process of the volumetric scroll pump has been performed. The analysis has been carried out with the Low-Reynolds number k-ε turbulence model under liquid hydrogen conditions. The study has been concentrated on the solution at the positions close to the end of the suction process. The present results agreed with the previous study. However, the solution shows that the improvements of the analytical model, *i.e.* cell patterns and time step give the qualitative enhancements comparing with the previous study.

It must be noted here that the maximum and minimum values of relative pressures increase and decrease significantly when the pockets move to close and separate fluid inside from suction chamber. This phenomenon might damage scroll pump components. Therefore, in the further study, to pre-

vent extremely high pressure and cavitations in real case, the pockets should open to the discharge chamber before they close and separate from the suction chamber.

References

1) P. Kritmaitree, *et al*., *J. Nucl. Sci. Technol.*, **37**[11], 996 (2000).
2) P. Kritmaitree, *et al*., *ICANS-XV*, Vol. 2, 1383 (2000).
3) Computational Dynamics Ltd., *STAR-CD User Guide Version 3.10*, 3–51 (1999).
4) F. S. Lien, *et al*., *Proc. 3rd Symp. on Eng. Turb. Model. & Meas.*, (1996).
5) B. E. Launder, D. B. Spalding, *Comp. Meth. Appl. Mech. Eng.*, **3**, 269 (1974).
6) W. Rodi, *Proc. 2nd Symp. on Turbulent Shear Flows*, (1979).
7) Computational Dynamics Ltd., *STAR-CD Methodology Version 3.10*, 7-2 (1999).